

High performance trench diamond JBS diode with a sidewall-enhanced structure

Ying Zhu(朱盈), Wang Lin(林旺), Dong-Shuai Li(李东帅), Liu-An Li(李柳暗), Xian-Yi Lv(吕宪义), Qi-Liang Wang(王启亮), and Guang-Tian Zou(邹广田)

Citation: Chin. Phys. B, 2023, 32 (**8**): 088101. DOI: 10.1088/1674-1056/acc2ae
Journal homepage: http://cpb.iphy.ac.cn; http://iopscience.iop.org/cpb

What follows is a list of articles you may be interested in

Suppression and compensation effect of oxygen on the behavior of heavily boron-doped diamond films

Li-Cai Hao(郝礼才), Zi-Ang Chen(陈子昂), Dong-Yang Liu(刘东阳), Wei-Kang Zhao(赵伟康),Ming Zhang(张鸣), Kun Tang(汤琨), Shun-Ming Zhu(朱顺明), Jian-Dong Ye(叶建东),Rong Zhang(张荣), You-Dou Zheng(郑有炓), and Shu-Lin Gu(顾书林)

Chin. Phys. B, 2023, 32 (**3**): 038101. DOI: 10.1088/1674-1056/ac7f8a

Effect of oxygen on regulation of properties of moderately boron-doped diamond films

Dong-Yang Liu(刘东阳), Li-Cai Hao(郝礼才), Wei-Kang Zhao(赵伟康), Zi-Ang Chen(陈子昂), Kun Tang(汤琨), Shun-Ming Zhu(朱顺明), Jian-Dong Ye(叶建东), Rong Zhang(张荣), You-Dou Zheng(郑有炓), and Shu-Lin Gu(顾书林)

Chin. Phys. B, 2022, 31 (**12**): 128104. DOI: 10.1088/1674-1056/ac8e96

One-dimensional sp carbon: Synthesis, properties, and modifications

Chao-Fan Lv(吕超凡), Xi-Gui Yang(杨西贵), and Chong-Xin Shan(单崇新)

Chin. Phys. B, 2022, 31 (**12**): 128103. DOI: 10.1088/1674-1056/ac872f

Determination of band alignment between GaO_x and boron doped diamond for a selective-area-doped termination structure

Qi-Liang Wang(王启亮), Shi-Yang Fu(付诗洋), Si-Han He(何思翰), Hai-Bo Zhang(张海波),Shao-Heng Cheng(成绍恒), Liu-An Li(李柳暗), and Hong-Dong Li(李红东)

Chin. Phys. B, 2022, 31 (**8**): 088104. DOI: 10.1088/1674-1056/ac464e

Synergistic influences of titanium, boron, and oxygen on large-size single-crystal diamond growth at high pressure and high temperature

Guang-Tong Zhou(周广通), Yu-Hu Mu(穆玉虎), Yuan-Wen Song(宋元文), Zhuang-Fei Zhang(张壮飞), Yue-Wen Zhang(张跃文), Wei-Xia Shen(沈维霞), Qian-Qian Wang(王倩倩), Biao Wan(万彪), Chao Fang(房超), Liang-Chao Chen(陈良超), Ya-Dong Li(李亚东), and Xiao-Peng Jia(贾晓鹏)

Chin. Phys. B, 2022, 31 (**6**): 068103. DOI: 10.1088/1674-1056/ac4650

High performance trench diamond junction barrier Schottky diode with a sidewall-enhanced structure

Ying Zhu(朱盈)[1,2], Wang Lin(林旺)[1,2], Dong-Shuai Li(李东帅)[1,2], Liu-An Li(李柳暗)[1,2], Xian-Yi Lv(吕宪义)[1,2], Qi-Liang Wang(王启亮)[1,2,†], and Guang-Tian Zou(邹广田)[1,2,‡]

[1] *State Key Laboratory of Superhard Materials, College of Physics, Jilin University, Changchun* 130012, *China*
[2] *Shenzhen Research Institute, Jilin University, Shenzhen* 518057, *China*

(Received 24 December 2022; revised manuscript received 25 February 2023; accepted manuscript online 9 March 2023)

The trench diamond junction barrier Schottky (JBS) diode with a sidewall enhanced structure is designed by Silvaco simulation. Comparing with the conventional trench JBS diode, Schottky contact areas are introduced on the sidewall of the trench beside the top cathode. The sidewall Schottky contact weakens the junction field-effect transistor effect between the trenches to realize a low on-resistance and a high Baliga's figure of merit (FOM) value. In addition, the existence of the n-type diamond helps to suppress the electric field crowding effect and enhance the reverse breakdown voltage. With the optimal parameters of device structure, a high Baliga's FOM value of 2.28 GW/cm^2 is designed. Therefore, the proposed sidewall-enhanced trench JBS diode is a promising component for the applications in diamond power electronics.

Keywords: diamond, Schottky barrier diode, junction terminal extension, simulation

PACS: 81.05.ug, 73.30.+y, 85.30.Kk, 88.30.gg **DOI:** 10.1088/1674-1056/acc2ae

1. Introduction

Diamond is a promising candidate for the next generation of high power and high frequency electronic applications due to its superior material properties, such as wide bandgap (5.5 eV), high breakdown electric field (> 10 MV·cm^{-1}), and high carrier mobility (4500 cm^2·V^{-1}·s^{-1} for electron, 3800 cm^2·V^{-1}·s^{-1} for hole).[1–4] The diamond-based Schottky barrier diodes (SBDs) play an essential role in industrial realms in virtue of the high-temperature durability (> 250 °C),[5,6] fast recovery,[7] high current (several to tens of amperes),[8] and high breakdown voltage.[9] However, the image force and electric field crowding effect under a relatively high reverse voltage increase the reverse leakage current and cause the premature breakdown. Until now, many kinds of termination structures such as junction termination extension, field plate, and junction barrier Schottky (JBS) have been adopted to alleviate the electric field crowding.[10,11]

The JBS diode is commonly used because it features the low turn-on voltage and fast switching frequency of a typical SBD,[12] as well as the high breakdown voltage of the integrated PN junction.[13] However, the junction depth of the n-type diamond formed by ion implantation is very shallow due to the high atom density and high hardness, which leads to the weak field shielding effect of diamond JBS diode. A trench JBS (T-JBS) structure that can realize a deeper pn junction than planar JBS is used to enhance the shield effect at Schottky contact interface.[14,15] On the other hand, the T-JBS diode introduces a strong depletion region along the sidewall of mesa between the trenches, which suppresses the forward current path and reduces the forward current density.[16,17] In previous work[18] a sidewall enhanced trench JBS (SET-JBS) SiC diode was proposed to increase the Schottky contact area and reduce the junction field-effect transistor (JFET) effect, resulting in the enhancement in forward current density and the specific on-resistance. However, it mainly focused on the forward current–voltage analytical model with mesa width as the parameter. Many other parameters such as doping concentration, trench depth, and regrowth process have not been evaluated extensively.

In this work, the influence of sidewall enhanced structure on the electrical performances of diamond JBS diode is investigated extensively and compared with that of the conventional trench JBS diode. The influences of structure parameters (the doping concentration, mesa width, trench depth, regrowth process) on forward and reverse properties of an SET-JBS diode are included in design through Silvaco simulation. The simulation results indicate that the proposed SET-JBS diode is promising component to balance the on-resistance (R_{on}) and the reverse breakdown voltage (V_{BD}). It demonstrates that the diamond-based JBS can reach a V_{BD} of approximately 1500 V and an R_{on} of approximately 1 mΩ·cm^2 by using only 3.0-μm-thick drift layer. On the other hand, the SiC SET-JBS requires 12-μm-thick drift layer to realize 1500 V and 3 mΩ·cm^2.[18]

†Corresponding author. E-mail: wangqiliang@jlu.edu.cn
‡Corresponding author. E-mail: gtzou@jlu.edu.cn

© 2023 Chinese Physical Society and IOP Publishing Ltd

2. Device structure and parameters

Figures 1(a)–1(c) show the device structures and parameters of the trenched SBD diode (T-SBD), the conventional T-JBS, and the proposed SET-JBS, respectively. The structure consists of three parts: the heavily doped p^+-diamond region (0.5 μm in thickness and 1×10^{19} cm^{-3} in hole density), the p^--diamond drift region (3 μm in thickness and 1×10^{16} cm^{-3} in hole density), and the n-diamond regions, which exist in the trenches. The Schottky (marked by red line) contact served as electrodes for different diode structures. The Schottky contact was defined by setting a work function to the metal while the ohmic contact is defined by default without a work function. To reveal the effect of pn junction, some key parameters such as the n-type doping concentration, mesa width (W_{mesa}), thickness of the n-type diamond ($T_{n\text{-}dia}$) and trench depth (D_{tr}) were evaluated. A series of n-type doping concentrations (1×10^{16} $cm^{-3}\sim10^{19}$ cm^{-3}), W_{mesa} (2 μm∼8 μm), and $T_{n\text{-}dia}$ (0.05 μm∼0.45 μm), as well as the D_{tr} (−0.3 μm∼0.1 μm) was adjusted to find the optimal Baliga's figure of merit (BFOM $= V_{BD}^2/R_{on}$). For the D_{tr}, the minus value means that the top surface of the n-type diamond is located underneath the surface of p^--diamond drift layer.

The main models used in our simulation were parallel-electric-field-dependent mobility model, the Auger recombination model, Shockley–Read–Hall model, and the impact ionization model. Finally, we calculate the R_{on} by using the current–voltage (I–V) curves, while the reverse V_{BD} was determined by the electric field distributions. Although the impact ionization model was added, the parameter values are different in many previous researches due to the premature breakdown of diamond material and device. Then, the JBS diode was deemed to be breakdown when the maximum electric field reached 6 MV/cm.[19,20]

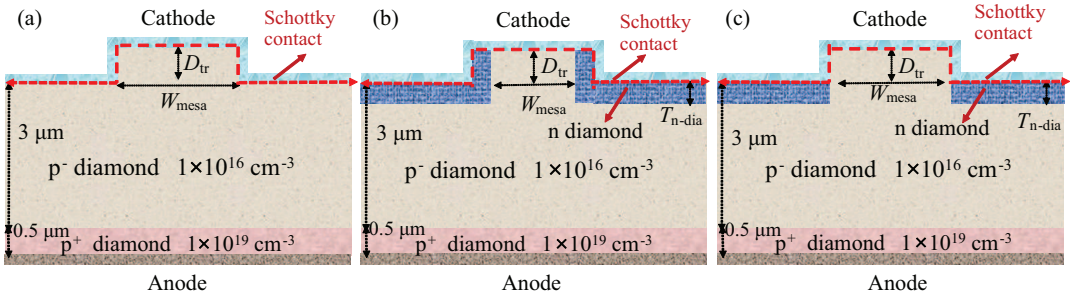


Fig. 1. Device structure and key parameters of (a) trench SBD diode, (b) conventional trench JBS diode, and (c) proposed sidewall enhanced trench JBS diode.

3. Results and discussion

Figure 2 shows the electrical characteristics of different diamond diodes obtained by TCAD simulation. For each of the three diodes, the W_{mesa}, $T_{n\text{-}dia}$, D_{tr}, and n-type diamond doping concentration are set to 6 μm, 0.15 μm, −0.2 μm, and 5×10^{17} cm^{-3}, respectively. It is observed from Fig. 2(a) that the forward I–V curve of the proposed SET-JBS diode presents a higher current density than that of the conventional T-JBS diode, but smaller than that of the T-SBD. The deduced R_{on} value is around 0.67 mΩ·cm^2 for the T-SBD structure, 0.86 mΩ·cm^2 for SET-JBS structure, and 1.46 mΩ·cm^2 for T-JBS structure. The current distributions of the diodes under a forward voltage of 4 V are also simulated to investigate the decreased R_{on} of SET-JBS (Fig. 2(c) and T-JBS (Fig. 2(d). Comparing with the conventional T-JBS, the proposed SET-JBS device has not only a larger Schottky contact area (in addition to the Schottky contact on the top cathode, the sidewall of the trenches also introduces Schottky contacts), but also a smaller JFET effect between the trenches. Thus, the forward current density increases but the R_{on} decreases.

The off-state electric field distributions of the diodes under −700 V are shown in Figs. 3(a)–3(c). The corresponding electric field profiles extracted along the cutline AA′ are plotted in Fig. 3(d). It is found that the trench structure in T-SBD can suppress the electric field localized beneath the Schottky electrode effectively, while two peaks are found at the mesa edges due to the electric field crowding phenomenon (Fig. 3(a)). The introduction of depletion regions by the pn junction helps to alleviate the electric field crowding and form a uniform distribution, resulting in an increased breakdown voltage (Figs. 3(b) and 3(c)). As shown in Fig. 3(d), the electric field of the conventional T-SBD diode is much higher than those of the other two diodes, which results in the highest leakage current density in all the diodes. The SET-JBS also alleviates the electric field crowding effectively. It is worth noting that the electric field at the Schottky contact of the proposed SET-JBS structure is slightly larger than that of T-JBS (Fig. 3(e)), which results in a slight amplitude of leakage current increase than the scenario in T-JBS. However, the electric field is still much smaller than that in the drift layer. It demonstrates that a maximum BFOM value of 1.96 GW/cm^2 is obtained in the proposed SET-JBS due to the better balance between the R_{on} and V_{BD}.

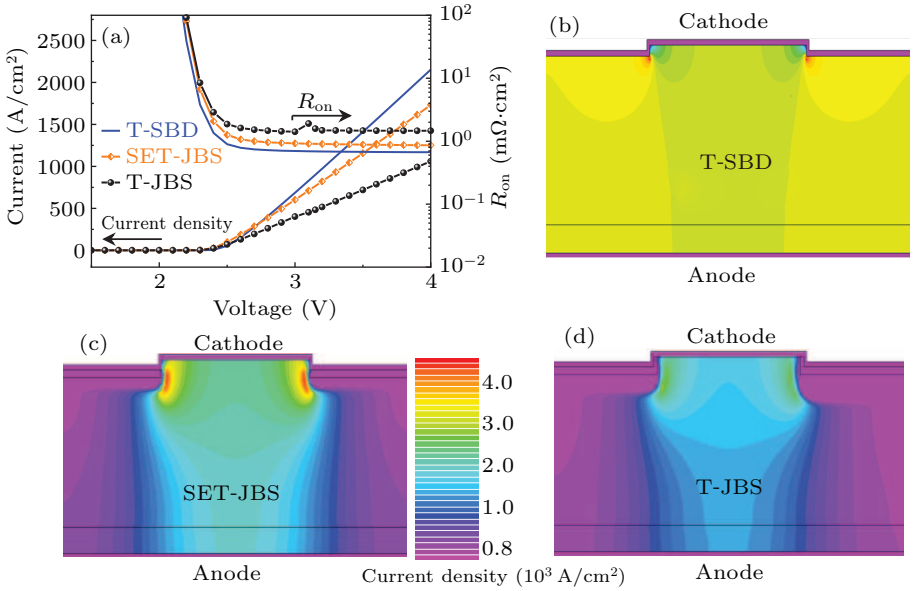


Fig. 2. (a) Linear forward *I*–*V* characteristics and corresponding R_{on} for three kinds of diodes, and (b)–(d) current density distribution under 4 V for the T-SBD diode, SET-JBS diode, and T-JBS diode, respectively.

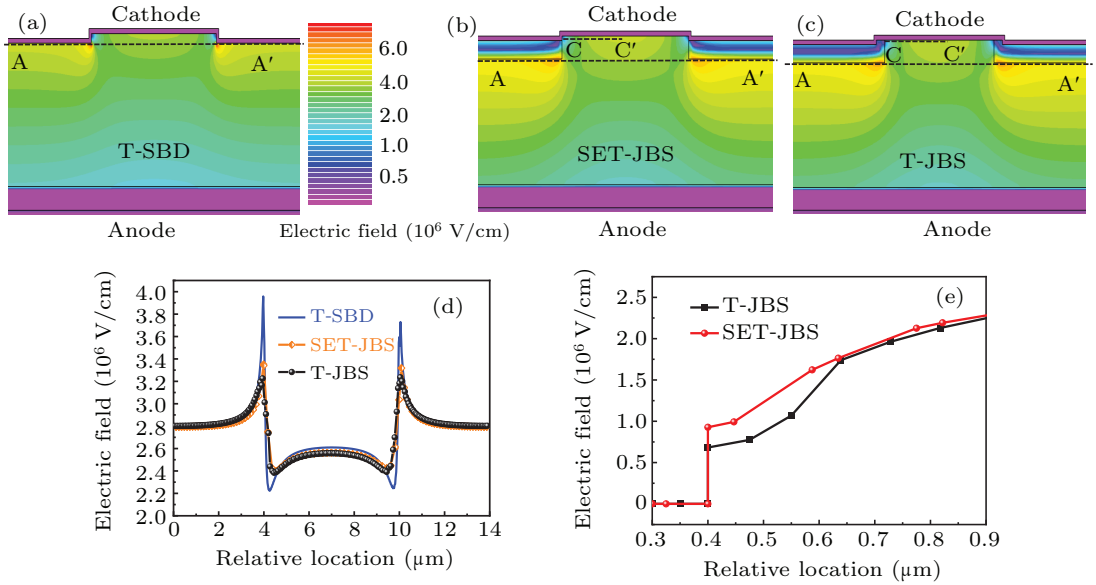


Fig. 3. Electric field distribution under −700 V for (a) T-SBD diode, (b) SET-JBS diode, and (c) T-JBS diode, respectively. (d)–(e) Electric field profiles obtained along cutline AA′ and CC′, respectively.

In the conventional JBS and T-JBS diode, the doping concentration of n-type region is a key parameter to modulate the electrical behaviors. Therefore, it is necessary to evaluate this parameter more detail. The W_{mesa}, $T_{n\text{-}dia}$, and D_{tr} of SET-JBS diode are set to 6 μm, 0.15 μm, and −0.2 μm, respectively. The resulting *I*–*V* curves show that the turn-on voltages are basically the same with doping concentration increasing, while the current density decreases slightly (as shown in Fig. 4(a)). As shown in Figs. 4(b)–4(f), the depletion region width of the pn junction becomes slightly wider and the Schottky contact area decreases with the augment of doping concentration, resulting in the slightly increased R_{on}. This result is consistent with our previous result.[21]

Moreover, the n-type diamond doping concentration of SET-JBS diode has an apparent effect on the electric field distributions (Figs. 5(a)–5(e)). Obviously, the n-diamond layer is totally depleted and the electric field concentrates around the edge of trench bottom when the doping concentration is lower than 5×10^{17} cm^{-3} (Figs. 5(a) and 5(b)). The electric distributions localized beneath the Schottky electrode and the pn junction tend to merge and form a much uniform one for a medium doping concentration (Figs. 5(c) and 5(d)). However, the electric field tends to crowd around the outer region of the n-type diamond region, resulting in a premature breakdown and the decrease of reverse breakdown voltage (Fig. 5(e)). The highest BFOM value of 1.96 GW/cm^2 is obtained for the sample with a doping concentration of 5×10^{17} cm^{-3}. Therefore, in the following discussion, we select the concentration of 5×10^{17} cm^{-3} for the n-type diamond doping concentration to realize high breakdown voltage (Fig. 5(f)).

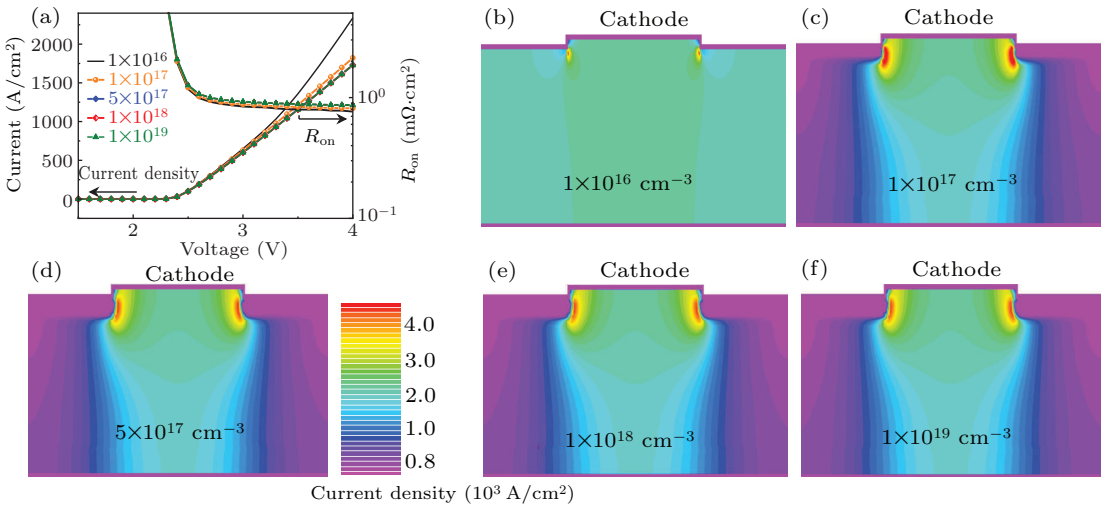


Fig. 4. (a) Linear forward *I*–*V* characteristics and the corresponding R_{on} for diodes with different doping concentrations, and (b)–(f) corresponding current density distributions under 4 V.

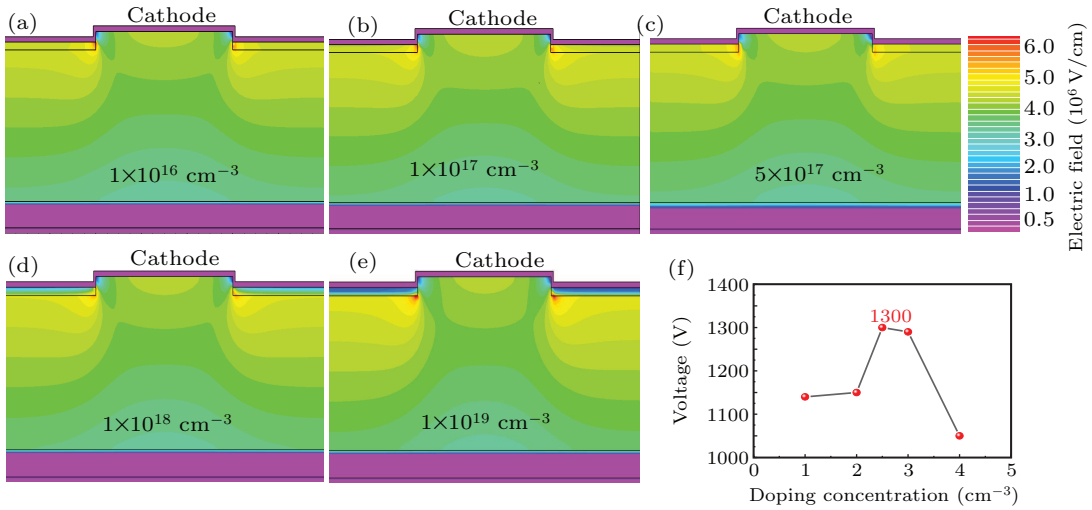


Fig. 5. (a)–(e) Electric field distributions under −1100 V for the SET-JBS diodes with different doping concentrations, (f) the corresponding breakdown voltage *versus* doping concentration. Numbers 1, 2, 2.5, 3, and 4 represent doping concentrations of 1×10^{16} cm^{-3}, 1×10^{17} cm^{-3}, 5×10^{17} cm^{-3}, 1×10^{18} cm^{-3}, and 1×10^{19} cm^{-3}, respectively.

In this section, we simulate the influence of W_{mesa} on the electrical characteristic of proposed SET-JBS diode. The n-type doping concentration, $T_{n\text{-}dia}$, and D_{tr} of SET-JBS diode are set to 5×10^{17} cm^{-3}, 0.15 μm, and −0.2 μm, respectively. The forward *I*–*V* characteristics for the proposed SET-JBS diode with different values of W_{mesa} (2 μm, 4 μm, 6 μm, and 8 μm) are shown in Fig. 6(a). It is shown that the current density increases and the R_{on} decreases slightly with W_{mesa} increasing, which can be ascribed to the increase of Schottky contact area (Figs. 6(c)–6(f)).

From the perspective of the off-state, the electric field profiles of the devices with different values of W_{mesa} are extracted along the cutline AA′ and plotted in Fig. 6(b). It is found that the W_{mesa} has no significant effect on the peak of electric field. However, the drift layer under Schottky contact can be shielded more effectively with a relatively smaller W_{mesa} (Fig. 6(g)). On the other hand, the electric fields under Schottky contact and pn junction tend to separate at a large W_{mesa} of 8 μm, deteriorating the uniformity of electric field distribution (Fig. 6(j)). Therefore, a high breakdown voltage of 1300 V and a high BFOM value of 1.96 GW/cm^2 are obtained at a W_{mesa} value of 6 μm.

The depletion regions play a key role in increasing the breakdown voltage. Therefore, the $T_{n\text{-}dia}$ needs to be optimized to achieve better electrical properties. The forward *I*–*V* characteristics with different $T_{n\text{-}dia}$ thickness values ($T_{n\text{-}dia}$ = 0.05 μm–0.45 μm) are shown in Fig. 7(a). It shows that the current density decreases slightly with the augment of $T_{n\text{-}dia}$. The main reason is that the depletion region of the pn junction suppresses the current conduction area with $T_{n\text{-}dia}$ increasing and resistance slightly increasing. On the other hand, obvious variation is observed on the electric field distribution under −1200 V for the SET-JBS diode with different values of $T_{n\text{-}dia}$ (Figs. 7(d)–7(f)), which can be confirmed from the profile extracted along the cutline AA′ (Fig. 7(b)). With the $T_{n\text{-}dia}$ increasing to 0.3 μm, the electric field crowding phenomenon

decreases somewhat, and the electric field distribution turns more uniform. The possible reason is that the width of depletion region increases with the augment of $T_{\text{n-dia}}$, which can attract the electric field and suppress the crowding around the Schottky edge. In the SET-JBS diode, the electric field distributes at the depletion regions of pn junctions and Schottky junctions. In addition, the depletion region of pn junctions is wider than that of the Schottky junctions and sustains stronger electric field. When the thickness is greater than 0.3 μm, the distance between the pn junction and the anode decreases. Then, the electric field tends to concentrate around the pn junction, resulting in the premature breakdown. Therefore, the electric field distribution is more uniform and the breakdown voltage reaches 1430 V at a $T_{\text{n-dia}}$ value of 0.3 μm (Fig. 7(c)), obtaining a high BFOM value of 2.27 GW/cm^2.

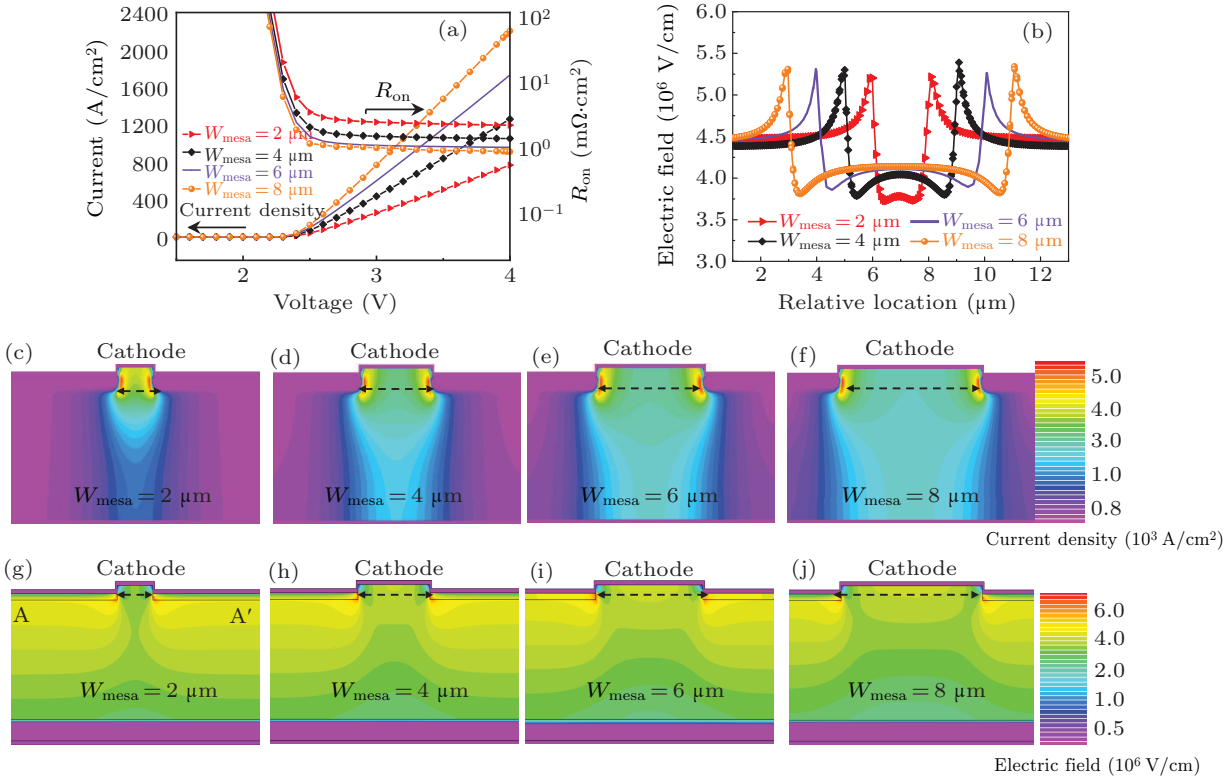


Fig. 6. (a) Linear forward *I*–*V* characteristics, (b) electric field profiles, (c)–(f) current density distributions at 4 V and (g)–(j) electric field distributions under −1200 V for diodes with different values of W_{mesa}.

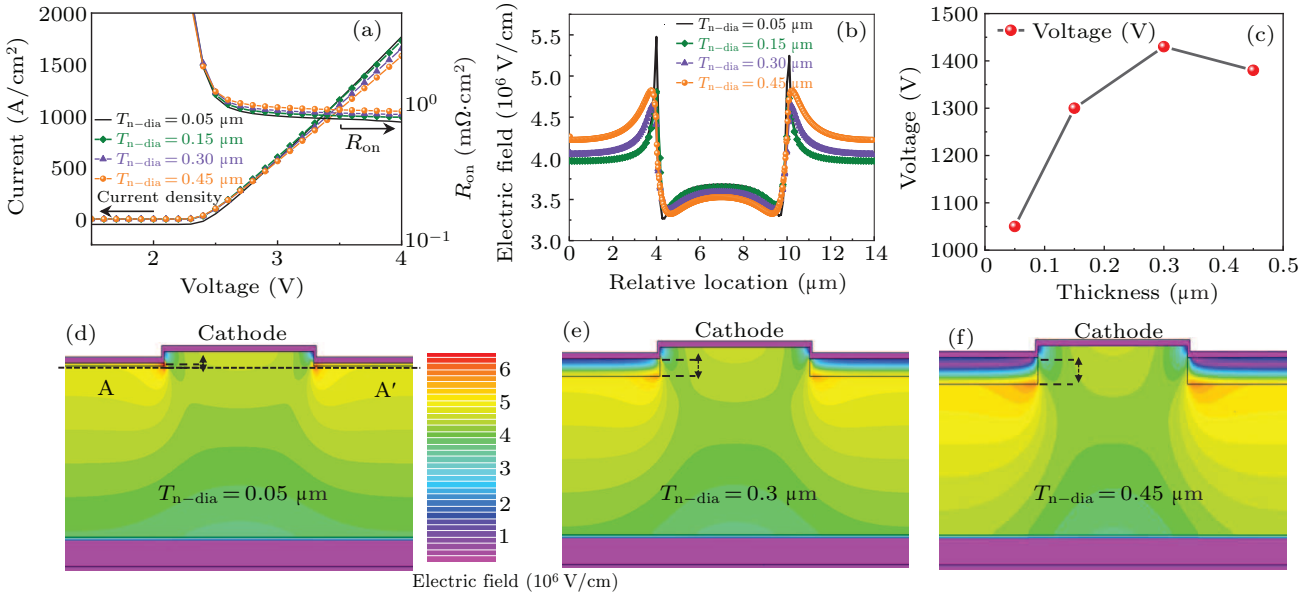


Fig. 7. (a) Linear forward *I*–*V* characteristics and the corresponding R_{on}, (b) electric field profiles under −1200 V, (c) breakdown voltage, and (d)–(f) electric field distributions under −1200 V for devices with different n-type-doped layer thickness values.

Considering the device fabrication process, the n-type diamond regions are regrown in the trench. Therefore, the device structure will be affected by the thickness of n-type diamond. A series of distances between n-diamond surface and the p-diamond surface ($D_{tr} = -0.3$, -0.2, -0.1, 0, and 0.1 μm) is used to further optimize the proposed SET-JBS diode structure. The n-type diamond doping concentration and W_{mesa} are 5×10^{17} cm^{-3} and 6 μm, respectively. As shown in Fig. 8(a), the current density decreases and the resistance increases slightly as the D_{tr} values change from negative to positive. The current density distributions at a forward bias of 4 V for different values of D_{tr} are shown in Figs. 8(b) and 8(c), demonstrating that the depletion region along sidewall spreads when the D_{tr} value changes, which will suppress the current conduction under Schottky contact. Furthermore, the reverse electric field distributions corresponding to different values of D_{tr} are extracted as shown in Figs. 9(a)–9(e). With the medium D_{tr} value of -0.1 μm, the crowding phenomenon (Fig. 9(a), $D_{tr} = -0.3$ μm) is alleviated and the electric field distribution is more uniform. A maximum breakdown voltage of 1480 V and a larger BFOM value of 2.28 GW/cm^2 are obtained (Fig. 9(f)). But when it is higher than -0.1 μm, the breakdown voltage of the device begins to decline. The possible reason can be given based on the electric field distribution in Figs. 9(a)–9(e). When the $D_{tr} = 0.1$ μm, the electric field distribution tends to concentrate around the corner of mesa, leading to premature breakdown and relatively small V_{BD}. The electric properties of the optimized SET-JBS are summarized in Table 1 to compare with those of typical T-JBS with the same dimensions, indicating the good potential of the proposed SET-JBS.

Table 1. Simulated electric characteristics for T-JBS and SET-JBS.

Device	V_{on} (V)	R_{on} (mΩ·cm^2)	V_{BD} (V)	BFOM (GW/cm^2)
T-JBS	2.1	1.33	1450	1.58
Optimized SET-JBS	2.2	0.96	1480	2.28

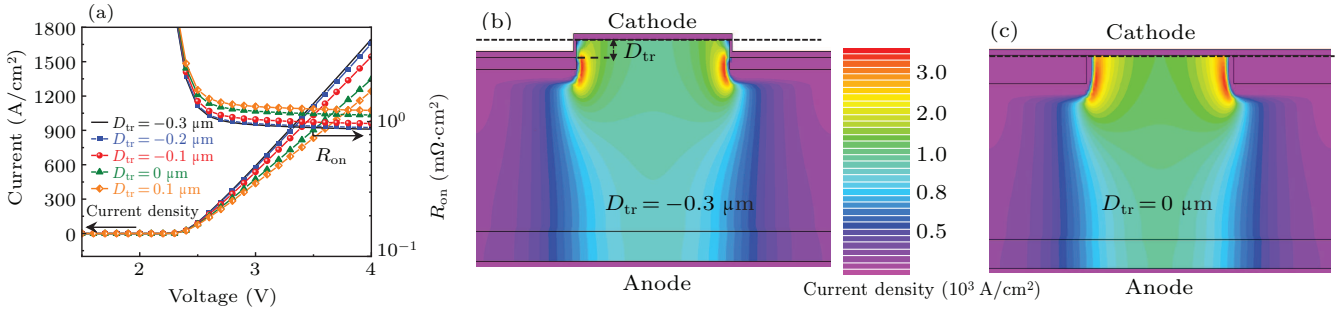


Fig. 8. (a) Linear forward *I*–*V* characteristics and the corresponding R_{on} for diodes with different trench depths, and typical current density distribution under 4 V for trench depth of (b) -0.3 μm and (c) 0 μm.

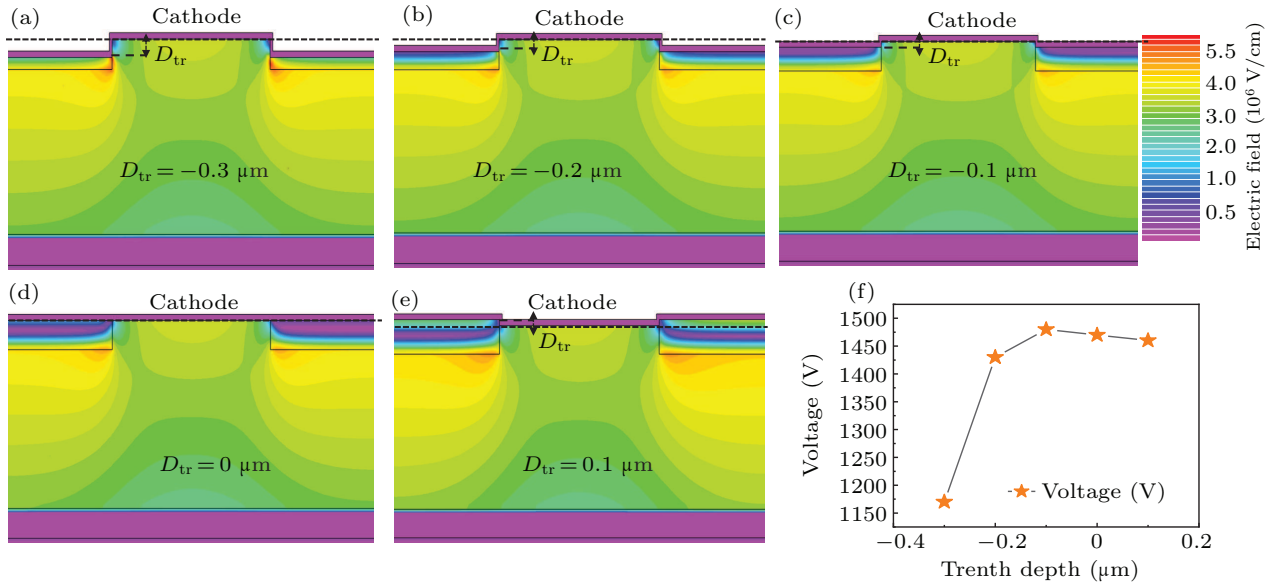


Fig. 9. (a)–(e) Electric field distributions under -1100 V for the proposed SET-JBS diode with different trench depths, and (f) relationship between breakdown voltage and trench depths.

4. Conclusions

In this work, a new trench JBS diode device (SET-JBS diode) is proposed to realize a high BFOM value. It demonstrates that the Schottky contact on the trench sidewall reduces the JFET effect in comparison with conventional trench JBS diode. The slight increase of Schottky contact area can in-

crease the current density and maintain a relatively high V_{BD}. Therefore, the proposed SET-JBS diode has the potential to replace the traditional T-JBS diode because of a better balance between the on-resistance and the breakdown voltage.

Furthermore, the effects of different structural parameters on the electrical properties of proposed diamond SET-JBS diode are discussed comprehensively. By optimizing the n-type diamond doping concentration (5×10^{17} cm^{-3}), mesa width ($W_{mesa} = 6$ μm), thickness of the n-type diamond ($T_{n\text{-}dia} = 0.3$ μm), and trench depth ($D_{tr} = -0.1$ μm), the electric field crowding is found to be significantly alleviated, resulting in more uniform distribution and higher breakdown voltage. The optimal SET-JBS structure shows a resistance of 0.96 mΩ·cm^2, breakdown voltage of 1480V, and BFOM value of 2.28 GW/cm^2.

Acknowledgements

Project supported by the Key Research and Development Program of Guangdong Province, China (Grant No. 2020B0101690001), the Natural Science Foundation of Sichuan Province, China (Grant No. 2022NSFSC0886), and the Open Project of State Key Laboratory of Superhard Materials, Jilin Province, China (Grant No. 202314).

References

[1] Kwak T, Lee J, Choi U, So B, Yoo G, Kim S and Nam O 2021 *Diamond Relat. Mater.* **114** 108335
[2] Wang J, Zhao D, Wang W, Zhang X, Wang Y, Chang X, Liu Z, Fu J, Wang K and Wang H X 2019 *Mater. Sci. Semicond. Process.* **97** 101
[3] Isberg J, Hammersberg J, Johansson E, Wikstrom T, Twitchen D J, Whitehead A J, Coe S E and Scarsbrook G A 2002 *Science* **297** 1670
[4] Zhao D, Liu Z, Wang J, Yi W, Wang R, Wang W, Wang K and Wang H X 2019 *Diamond Relat. Mater.* **99** 107529
[5] Ueda K, Kawamoto K and Asano H 2014 *Jpn. J. Appl. Phys.* **53** 04EP05
[6] Hanada T, Ohmagari S, Kaneko J H and Umezawa H 2020 *Appl. Phys. Lett.* **117** 262107
[7] Twitchen D J, Whitehead A J, Coe S E, Isberg J, Hammersberg J, Wikstrom T and Johansson E 2004 *IEEE Trans. Electron Dev.* **51** 826
[8] Tarelkin S, Bormashov V, Buga S, Volkov A, Teteruk D, Kornilov N, Kuznetsov M, Terentiev S, Golovanov A and Blank V 2015 *Phys. Status Solidi A* **212** 2621
[9] Butler J E, Geis M W, Krohn K E, Lawless J, Deneault S, Lyszczarz T M, Flechtner D and Wright R 2003 *Semicond. Sci. Technol.* **18** S67
[10] Driche K, Rugen S, Kaminski N, Umezawa H, Okumura H and Gheeraert E 2018 *Diamond Relat. Mater.* **82** 160
[11] Hull B A, Sumakeris J J, O'Loughlin M J, Zhang Q, Richmond J, Powell A R, Imhoff E A, Hobart K D, Rivera-Lopez A and Hefner A R 2008 *IEEE Trans. Electron Dev.* **55** 1864
[12] Kobayashi A, Ohmagari S, Umezawa H, Takeuchi D and Saito T 2020 *Jpn. J. Appl. Phys.* **59** 089302
[13] Song Q W, Zhang Y M, Zhang Y M, Chen F P and Tang X Y 2011 *Chin. Phys. B* **20** 057301
[14] Konishi K, Kameshiro N, Yokoyama N, Shima A and Shimamoto Y 2017 *Jpn. J. Appl. Phys.* **56** 121301
[15] Wu L, Lei B, Yang H, Song Y and Zhang Y 2018 *Superlattices Microstruct.* **123** 201
[16] Ren N, Wu J, Liu L and Sheng K 2020 *IEEE Trans. Electron Dev.* **35** 11316
[17] Radhakrishnan R, Cueva N, Witt T and Woodin R L 2018 *Mater. Sci. Forum* **924** 621
[18] Kong M, Chen Z, Gao J, Duan Y, Hu Z, Yi B and Yang H 2022 *Semicond. Sci. Technol.* **37** 075008
[19] Wang Q L, Wang T T, Pu T F, Cheng S C, Li X B, Li LA and Ao J P 2022 *Chin. Phys. B* **31** 057702
[20] Lin W, Wang T T, Wang Q L, Lv X Y, Li G Z, Li L A, Ao J P and Zou G T 2022 *Chin. Phys. B* **31** 108105
[21] Li D, Wang T, Lin W, Zhu Y, Wang Q, Lv X, Li L and Zou G 2022 *Diamond Relat. Mater.* **128** 109300